First-principles correction scheme for linear-response time-dependent density functional theory calculations of core electronic states

Bussy, Augustin ; Hutter, Jürg

DOI: https://doi.org/10.1063/5.0058124

The Journal of Chemical Physics

First-principles correction scheme for linear-response time-dependent density functional theory calculations of core electronic states

Cite as: J. Chem. Phys. **155**, 034108 (2021); https://doi.org/10.1063/5.0058124
Submitted: 27 May 2021 • Accepted: 30 June 2021 • Published Online: 15 July 2021

Augustin Bussy and Jürg Hutter

The Journal of Chemical Physics ARTICLE scitation.org/journal/jcp

First-principles correction scheme for linear-response time-dependent density functional theory calculations of core electronic states

Cite as: J. Chem. Phys. 155, 034108 (2021); doi: 10.1063/5.0058124
Submitted: 27 May 2021 • Accepted: 30 June 2021 •
Published Online: 15 July 2021

Augustin Bussy[a] and Jürg Hutter[b]

AFFILIATIONS

Department of Chemistry, University of Zurich, Winterthurerstrasse 190, CH-8057 Zürich, Switzerland

[a]**Current address:** Department of Chemistry, University of Zurich, Winterthurerstrasse 190, CH-8057 Zürich, Switzerland.
Author to whom correspondence should be addressed: augustin.bussy@chem.uzh.ch
[b]**Electronic mail:** hutter@chem.uzh.ch

ABSTRACT

Linear-response time-dependent density functional theory (LR-TDDFT) for core level spectroscopy using standard local functionals suffers from self-interaction error and a lack of orbital relaxation upon creation of the core hole. As a result, LR-TDDFT calculated x-ray absorption near edge structure spectra needed to be shifted along the energy axis to match experimental data. We propose a correction scheme based on many-body perturbation theory to calculate the shift from first-principles. The ionization potential of the core donor state is first computed and then substituted for the corresponding Kohn–Sham orbital energy, thus emulating Koopmans's condition. Both self-interaction error and orbital relaxation are taken into account. The method exploits the localized nature of core states for efficiency and integrates seamlessly in our previous implementation of core level LR-TDDFT, yielding corrected spectra in a single calculation. We benchmark the correction scheme on molecules at the K- and L-edges as well as for core binding energies and report accuracies comparable to higher order methods. We also demonstrate applicability in large and extended systems and discuss efficient approximations.

I. INTRODUCTION

X-ray absorption spectroscopy (XAS) is a major characterization tool used in many fields of natural science. The technique provides a local and element specific probe, yielding insights into the geometric and electronic structure of matter. In particular, the x-ray absorption near edge structure (XANES) region of the spectrum holds information about the chemical state (coordination number, oxidation state, and so on) of the probed atom. As technology progresses and quality light sources become more accessible, XANES is used increasingly often. Following this trend, many theoretical approaches have been developed to help interpret experiments.

One of the most widespread computational methods for the simulation of XANES is time-dependent density functional theory (TDDFT). It offers a favorable trade-off between cost and accuracy and is relatively easy to use due to its mostly "black-box" nature. In its standard formulation,[1,2] TDDFT is best suited for UV–vis spectroscopy, where electronic transitions from valence to low lying unoccupied bound states take place. Much effort has been made in adapting the theory to core state spectroscopy. Most notably, core–valence separation[3] (CVS) has been used with both flavors of TDDFT, real-time[4] (RT-TDDFT) and linear-response[5–7] (LR-TDDFT), allowing for the calculation of excitations from core states at an affordable cost. Other approaches rely on iterative solvers, which can directly target high energy core transitions,[8,9] thus bypassing the CVS. The different implementations yield consistent results, and the choice of the exchange–correlation functional typically has a larger impact on accuracy.[10]

While TDDFT generated XANES spectra are known to have accurate relative feature intensities and spacing, they usually have to be translated along the energy axis to match experiments. The main reasons behind this shortcoming of TDDFT lie in the lack of orbital

relaxation upon the creation of a core hole and self-interaction errors[11] (SIEs). There are multiple ways of dealing with these issues. The simplest is to apply a system dependent empirical shift,[12–14] although this limits TDDFT to a purely descriptive role. Similarly, an atom specific shift can be calibrated over multiple systems to be later applied to similar calculations.[15,16] A common approach to computing the shift from first-principles is by performing a separate ΔSCF[10,17] calculation. By taking the difference between the converged ground and first excited states' total energies, SIE mostly cancels out and orbital relaxation is taken into account. However, such calculations may be hard to set up and converge. Other techniques have been proposed to tackle SIE in TDDFT, for example, by basing the TDDFT calculation on a SIE corrected ground state calculation,[11,18] fitting the fraction of Hartree–Fock exchange in hybrid functionals,[6] or developing core TDDFT specific functionals[19–21] (usually relying on empirically fitted parameters). For calculations involving excitations from heavy atoms, scalar relativistic effects do also play a role. This is usually taken into account at the ground state level using the ZORA[22] or DKH[23] approach.

In this work, we propose a fully *ab initio* correction scheme for core LR-TDDFT spectroscopy based on many-body perturbation theory. The method exploits the localized nature of core states for efficiency and seamlessly integrates into our previous implementation of core LR-TDDFT[24] in the CP2K software package.[25] The method accounts for orbital relaxation and self-interaction error while yielding the core ionization potential as a side-product. We discuss the method's implementation and demonstrate its applicability to molecules at the K- and L-edges and as a means of calculating core binding energies. We also discuss efficient approximations and applications in extended systems.

II. THEORY

The LR-TDDFT equations are built on the solutions of the time-independent Kohn–Sham (KS) equations. Expanded in a basis of atom-centered functions, the KS orbitals read

$$\phi_{i\sigma}(\mathbf{r}) = \sum_p c^0_{pi\sigma}\varphi_p(\mathbf{r}), \tag{1}$$

where the basis elements $\{\varphi_p(\mathbf{r})\}$, also referred to as atomic orbitals (AOs), are typically non-orthogonal Gaussian type orbitals (GTOs) with

$$S_{pq} = \langle\varphi_p|\varphi_q\rangle. \tag{2}$$

Note that throughout this work, indices $p, q, \ldots$, always refer to AOs; $i, j, \ldots$, refer to occupied MOs; $a, b, \ldots$, refer to virtual MOs; and $\sigma, \tau, \ldots$ refer to spin.

In the Sternheimer[26,27] approach to LR-TDDFT, vertical excitation energies are obtained by solving the non-Hermitian eigenvalue equation[24]

$$\omega\begin{pmatrix}-\mathbf{G} & 0\\ 0 & \mathbf{G}\end{pmatrix}\begin{pmatrix}\mathbf{c}^+\\ \mathbf{c}^-\end{pmatrix} = \begin{pmatrix}\mathbf{A}+\mathbf{B}-\mathbf{D} & \mathbf{B}-\mathbf{E}\\ \mathbf{B}-\mathbf{E} & \mathbf{A}+\mathbf{B}-\mathbf{D}\end{pmatrix}\begin{pmatrix}\mathbf{c}^+\\ \mathbf{c}^-\end{pmatrix}, \tag{3}$$

where the $\mathbf{c}^\pm$ eigenvectors are the coefficients for the basis expansion of the LR orbitals and ω is the corresponding excitation energy. The matrix $\mathbf{G}$ is related to the basis set overlap,

$$G_{pi\sigma,qj\tau} = S_{pq}\delta_{ij}\delta_{\sigma\tau}, \tag{4}$$

and the matrix $\mathbf{A}$ is based on the ground state KS matrix $\mathbf{F}^\sigma$,

$$A_{pi\sigma,qj\tau} = \left(F^\sigma_{pq} - \varepsilon_{i\sigma}S_{pq}\right)\delta_{ij}\delta_{\sigma\tau}, \tag{5}$$

where $\varepsilon_{i\sigma}$ is the KS eigenvalue and $\mathbf{B}$, $\mathbf{D}$, and $\mathbf{E}$ are the Hartree exchange–correlation kernel and on- and off-diagonal Hartree–Fock (HF) exchange kernel matrices,

$$B_{pi\sigma,qj\tau} = \sum_{rs} Q^\sigma_{pr}(ri_\sigma|f^{Hxc}_{\sigma,\tau}|sj_\tau)Q^\tau_{qs}, \tag{6}$$

$$D_{pi\sigma,qj\tau} = c_{\mathrm{HF}}\ \delta_{\sigma\tau}\sum_{rs} Q^\sigma_{pr}(rs|i_\sigma j_\tau)Q^\tau_{qs}, \tag{7}$$

$$E_{pi\sigma,qj\tau} = c_{\mathrm{HF}}\ \delta_{\sigma\tau}\sum_{rs} Q^\sigma_{pr}(rj_\tau|si_\sigma)Q^\tau_{qs}, \tag{8}$$

where $\mathbf{Q}^\sigma$ is a projector on the unoccupied unperturbed space, C_{HF} is the fraction of HF exchange, and $f^{Hxc}_{\sigma,\tau}$ is defined as

$$f^{Hxc}_{\sigma,\tau}(\mathbf{r},\mathbf{r}') = \frac{1}{|\mathbf{r}-\mathbf{r}'|} + \left.\frac{\delta^2 E_{xc}}{\delta n_\sigma(\mathbf{r})\delta n_\tau(\mathbf{r}')}\right|_{n^0} \tag{9}$$

within the adiabatic approximation.[28]

The eigenvalue equation can be greatly simplified by setting $\mathbf{c}^+ = 0$ while retaining the eigenvalue accuracy.[29] This reduces the matrix dimensions by a factor of 2 and allows ignoring the off-diagonal exact exchange kernel matrix $\mathbf{E}$. This is known as the Tamm–Dancoff approximation[30] (TDA) and is consistently applied throughout this work.

When dealing with core-spectroscopy, specific approximations can be made for efficiency. First, core and valence excitations can be effectively decoupled within the CVS, allowing the neglect of the latter.[3] Because core MOs are systematically involved in the repulsion integrals (ERIs) to be evaluated, additional screening can take place[31] and the related cost is lowered. The dimension of the eigenvalue problem in Eq. (3) is reduced as well, bringing down the cost of diagonalization. Moreover, core states of interests can be treated serially within the sudden approximation,[7,32] further reducing matrix dimensions to that of the ground state KS matrix. In this context, all the four-center ERIs needed for the kernel matrices have either the form $(pI|qJ)$ or $(pq|IJ)$, where ϕ_I and ϕ_J are core donor MOs. In our recent implementation[24] of core level LR-TDDFT in the CP2K software package,[25] we introduced a local resolution of the identity (RI) scheme that further reduces the cost of ERIs,

$$(pI|qJ) \approx \sum_{\mu,\nu}(pI|\mu)\ (\mu|\nu)^{-1}\ (\nu|qJ) \tag{10}$$

and

$$(pq|IJ) \approx \sum_{\mu,\nu}(pq|\mu)\ (\mu|\nu)^{-1}\ (\nu|IJ), \tag{11}$$

where the RI basis $\{\chi_\mu(\mathbf{r})\}$ only consists of Gaussian functions centered on the excited atom. Such a choice of basis is only possible due to the localized nature of core states. In the case of K-edge spectroscopy, only the 1s core MO is considered. For the $L_{2,3}$-edge, the core MOs span all three 2p states.

LR-TDDFT yields excitation energies as corrections to ground state orbital energy differences,[43] i.e.,

$$\omega = \varepsilon_a - \varepsilon_I + \Delta_{xc}, \tag{12}$$

where ε_a is the orbital energy of a virtual receiving MO and ε_I is that of the core donor MO. Under Koopmans's condition, ε_a and ε_I are identified as the electron affinity (EA) and the negative ionization potential (IP), respectively. However, mostly because of the self-interaction error, DFT orbital energies are far from the actual EAs and IPs and the condition does not hold.[44] Nonetheless, and especially since $|\varepsilon_I| \gg |\varepsilon_a|$, absolute LR-TDDFT core excitation energies are expected to be greatly improved if $-\varepsilon_I$ were to be substituted by an accurate value of the core IP in Eq. (5). This leads to a rigid shift of the spectrum, while the LR-TDDFT relative energies and intensities are preserved. A similar approach was developed by Verma and Bartlett,[45] where an IP corrected exchange–correlation potential was designed and successfully applied. In the current work, the focus is on the correction of a single core IP using many-body perturbation theory, regardless of the chosen exchange–correlation functional.

Based on a Hartree–Fock ground state calculation, ionization potentials can be computed using second-order electron propagator theory[46,47] by solving the following equation:

$$\mathrm{IP}_I = -\varepsilon_I - \frac{1}{2}\sum_{ajk}\frac{|\langle Ia||jk\rangle|^2}{-\mathrm{IP}_I + \varepsilon_a - \varepsilon_j - \varepsilon_k} - \frac{1}{2}\sum_{abj}\frac{|\langle Ij||ab\rangle|^2}{-\mathrm{IP}_I + \varepsilon_j - \varepsilon_a - \varepsilon_b}, \tag{13}$$

where indices a and b refer to virtual orbitals and j and k refer to occupied HF spin-orbitals. Note that the antisymmetrized four-center integrals $\langle Ia||jk\rangle$ and $\langle Ij||ab\rangle$ systematically involve the spin-orbital for which the IP is computed. Equation (13) can be formally adapted to a DFT reference by constructing the generalized Fock matrix based on the KS orbitals. The occupied and virtual orbitals are then separately rotated such that they become canonical with respect to the generalized Fock matrix. These pseudocanonical orbitals and corresponding new eigenvalues are then used in Eq. (13). This is known as the GW2X method.[48] Alternatively, we also propose the GW2X* method, in which KS orbitals are directly used,

$$\mathrm{IP}_I^{\mathrm{GW2X}^*} = -f_{II} - \frac{1}{2}\sum_{ajk}\frac{|\langle Ia||jk\rangle|^2}{-\mathrm{IP}_I + f_{aa} - f_{jj} - f_{kk}} - \frac{1}{2}\sum_{abj}\frac{|\langle Ij||ab\rangle|^2}{-\mathrm{IP}_I + f_{jj} - f_{aa} - f_{bb}}, \tag{14}$$

where f_{II} is the diagonal element of the generalized Fock matrix corresponding to the ϕ_I KS orbital. This approach has an efficiency advantage over the original GW2X as potentially expensive orbital rotations are avoided. Its implementation is also simpler. The second-order electron propagator method accounts for relaxation effects upon creation of the core hole as well as electron correlation.[49] Moreover, it is free of self-interaction error since the generalized Fock matrix, which is built with 100% exact exchange, is used. Finally, this is a fully *ab initio* scheme that does not rely on any empirical parameter.

Both GW2X and GW2X* methods were implemented in CP2K, where they can be employed as a correction scheme for core level LR-TDDFT and/or a way of computing core ionization potentials for x-ray photoelectron spectroscopy (XPS). For each excited core state ϕ_I in the system, the RI three-center ERIs $(pq|\nu)$ and $(\mu|rI)$ are first computed. It is followed by contraction steps from AOs to MOs such that the anti-symmetrized ERIs needed in Eq. (13) or Eq. (14) can be constructed. The electron propagator equation is then solved using a Newton–Raphson scheme, and the resulting IP is substituted into Eq. (5). From there, the normal LR-TDDFT problem is solved, reusing the precomputed ERIs $(pq|\nu)$ and $(\mu|rI)$. Note that the size of the RI basis $\{\chi_\mu(\mathbf{r})\}$ is independent of the system size. Hence, storing $(pq|\mu)$ scales as $\mathcal{O}(n^2)$ in memory at worst. Moreover, contracting $(pq|\mu)$ to, e.g., $(ab|\mu)$ has the same computational scaling as a normal matrix–matrix multiplication, namely, $\mathcal{O}(n^3)$. Since MOs are not localized, storing a fully contracted tensor $(ab|Ij)$ would scale cubically in memory. This can be avoided by contracting $(ab|\mu)$ and $(\nu|Ij)$ first and leaving the RI contraction as the last step. The final contraction can then be done in batches, and the $(ab|Ij)$ integrals are never fully stored. All integral storage and contraction are done using the sparse matrix and tensor library DBCSR.[60]

III. BENCHMARKS AND RESULTS

The implementation of the GW2X method for core states is tested on a wide range of systems, functionals, and basis sets. Benchmarks cover GW2X as a correction to LR-TDDFT for K- and L-edge spectroscopy and as a mean of calculating ionization potentials. We investigate basis set convergence and compare the method to literature benchmarks for molecules. We also discuss the impact of various approximations on accuracy and apply the method to extended systems in periodic boundary conditions.

A. GW2X as correction to LR-TDDFT

To assess the applicability of the GW2X method as a correction to core LR-TDDFT, we calculated the first K-edge excitation energy of 25 molecules with first and second row atoms and compared to experimental data. The benchmark set includes 16 distinct excitations from molecular C1s levels, 10 from N1s, 13 from O1s, and 4 from F1s. The structures were optimized at the def2-TZVP[61]/B3LYP[62] level. For this benchmark, we used the core-specific aug-pcX basis set[63] and four common hybrid functionals with increasing fraction of Hartree–Fock exchange [B3LYP (20%), PBE0 (25%),[64] PBEh (45%),[65] and BHHLYP (50%)].[66] In Fig. 1, the mean absolute deviation (MAD) of LR-TDDFT and LR-TDDFT+GW2X first excitation energies with respect to experiments is displayed for different functional and basis set combinations. The GW2X correction systematically improves the LR-TDDFT results and brings down the very disparate MADs of the different functionals to a similar level. This can be explained by the fact that a higher HFX fraction leads to a reduction in the self-interaction error, whereas the GW2X correction is free of it altogether. It can also be observed that increasing the basis set quality from double to quadruple zeta quality does not significantly change the results,

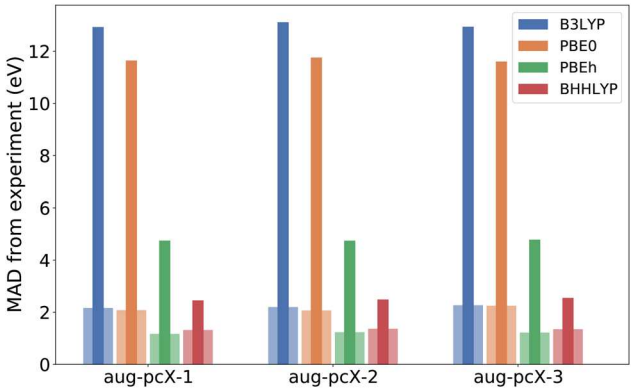

FIG. 1. Mean absolute deviation of the first K-edge excitation energy calculated using pure LR-TDDFT (thin dark bars) and GW2X corrected LR-TDDFT (wide clear bars) with respect to experimental values. The benchmark set is made of 25 first and second row atom molecules and covers 43 distinct excitations.

suggesting rapid convergence. Finally, the GW2X corrected PBEh(α = 0.45) functional performs the best overall with MADs of 1.32, 1.38, and 1.37 eV for the aug-pcX-1, aug-pcX-2, and aug-pcX-3 basis sets, respectively. A detailed table containing the calculated and reference energies for each molecule is available in the supplementary material.

In Table I, LR-TDDFT with GW2X correction is compared to other XANES K-edge calculation methods reported in the literature. A smaller selection of nine molecules (12 excitations) was made such as to maximize overlap with the other studies. The aug-pcX-2 basis (triple zeta quality) was chosen for similar reasons, and the PBEh (α = 0.45) functional was selected because it performed best in the previous benchmark. Note that the reported MADs can only be used as the semi-quantitative measure of method quality because of the small sample size, patchy data, and varying basis sets. GW2X corrected LR-TDDFT performs on par with B3LYP-ΔSCF and equation of motion CCSD while surpassing CIS(D). SRC2-TDDFT performs better, but the core-specific range separated SRC2 functional has four parameters, which were specifically fitted on those molecules.[21] Finally, the square gradient minimization (SGM) method developed by Hait and Head-Gordon[73] combined with ROKS and the SCAN[74] functional also yields better results. However, both LR-TDDFT and GW2X correction schemes can be applied without prior knowledge of a target system, whereas SGM requires careful preparation of an initial guess. This "black-box" aspect of LR-TDDFT+GW2X makes it an interesting method for high-throughput studies.

GW2X can be used to correct XANES LR-TDDFT at the L-edge, where the ionization potential of the three 2p states is computed and spin–orbit coupling is included at the TDDFT level. It is, however, necessary to compare calculated and experimental spectra to reliably extract the first excitation energies at the L_2 and L_3 peaks, making large scale benchmark studies difficult. Instead, we focus on a few molecules present in similar studies and compare results in Table II. Geometries were optimized at the def2-TZVP/B3LYP level and the PBEh(α = 0.45) functional with the aug-pcX-2 basis chosen for the LR-TDDFT+GW2X calculations. All three methods perform similarly well, both at the L_2 and L_3 peaks and with errors comparable to those observed at the K-edge. Note that on average, the GW2X correction induces a blue shift of 2.4 eV compared to bare LR-TDDFT, again systematically improving the results. The amount of spin–orbit splitting is well captured by all three methods.

B. GW2X for core IP calculations

GW2X can also be used as a stand-alone method to compute ionization potentials. In this case, all TDDFT related operations can be ignored for efficiency. Alternatively, the IPs can be obtained as a side-product of a corrected LR-TDDFT calculation. To assess the quality of GW2X in this context, the CORE65 benchmark set[67] was used. It contains 65 distinct core states over 32 molecules with

TABLE I. Comparison of GW2X corrected LR-TDDFT for XANES K-edge spectroscopy with similar methods from the literature. The difference between the calculated and experimental first allowed excitation is reported (in eV). The bold atom in the chemical formula is the one from which the excitation takes place.

	B3LYP-ΔSCF[33] u6-311(2+,2+)G**	SCAN-ROKS[34] aug-cc-pCVTZ	SRC2-TDDFT[21] 6-311(2+,2+)G**	CIS(D)[35] aug-cc-pCVQZ	EOM-CCSD[36] aug-cc-pCVTZ[a]	PBEh-GW2X aug-pcX-2	Expt.
CH_4	+0.5	0.0	⋯	+0.3	⋯	+0.9	288.0[37]
C$_2H_4$	⋯	0.0	+0.6	⋯	+1.8	+1.2	284.7[38]
CO	−0.8	−0.4	−0.7	+2.5	−0.4	+2.5	287.4[39]
CH_2O	−0.1	⋯	0.0	+2.8	⋯	+1.7	286.0[40]
NH_3	⋯	−0.5	⋯	⋯	+0.1	+0.9	400.8[37]
NNO	−0.7	−0.1	⋯	+2.4	⋯	+0.2	401.0[41]
N**N**O	−0.8	−0.2	⋯	+2.8	⋯	+0.4	404.6[41]
C**O**	−0.6	−0.3	0.0	−0.5	+0.4	−0.7	534.2[39]
H_2**O**	⋯	⋯	⋯	⋯	+0.4	−0.1	534.0[37]
CH_2**O**	−0.4	⋯	0.0	+1.0	⋯	−1.1	530.8[40]
H**F**	⋯	−0.3	−0.5	⋯	+0.4	−0.8	687.4[42]
F_2	⋯	−0.2	⋯	⋯	⋯	−0.7	682.2[42]
MAD	0.6	0.2	0.3	1.8	0.6	0.9	

[a]With additional Rydberg functions.

TABLE II. Comparison of GW2X corrected LR-TDDFT for XANES L-edge spectroscopy with similar methods from the literature. The difference between the calculated and experimental first excitation at the L_2- and L_3-edge is reported (in eV). All methods include relativistic treatments for the spin–orbit coupling. The bold atom in the chemical formula is the one from which the excitation takes place.

	L_3				L_2			
	SCAN-ROKS[34] aug-cc-pCVTZ	EOM-CCSD[50] uC-6-311(2+,+)G**	PBEh-GW2X aug-pcX-2	Expt.	SCAN-ROKS[34] aug-cc-pCVTZ	EOM-CCSD[50] uC-6-311(2+,+)G**	PBEh-GW2X aug-pcX-2	Expt.
SiH_4	+0.4	−0.3	+1.2	102.6[51]	+0.4	−0.3	+1.1	103.2[51]
SiCl_4	+0.3	⋯	−0.4	104.2[52]	+0.3	⋯	−0.3	104.8[52]
PH_3	+0.2	⋯	+0.4	131.9[53]	+0.1	⋯	+0.5	132.8[53]
PF_3	0.0	⋯	+0.2	134.9[54]	+0.1	⋯	+0.5	135.6[54]
H_2**S**	+0.3	−0.2	+0.3	164.4[55]	+0.3	−0.1	+0.2	165.6[55]
OC**S**	+0.1	+0.1	+0.1	164.3[56]	+0.2	−0.1	+0.2	165.5[56]
SO_2	⋯	+0.1	0.0	164.4[57]	⋯	+0.3	+0.2	165.6[57]
H**Cl**	+0.1	⋯	+0.4	200.9[58]	+0.2	⋯	+0.6	202.4[58]
Cl$_2$	0.0	⋯	−0.6	198.2[59]	+0.1	⋯	−0.5	199.8[59]
MAD	0.2	0.2	0.4		0.2	0.2	0.4	

first and second row atoms, covering 30 C1s, 21 O1s, 11 N1s, and 3 F1s. Core ionization potentials were calculated with the B3LYP, PBE0, PBEh(α = 0.45), and BHHLYP functionals and the aug-pcX basis sets. Mean average deviations from experiments are displayed in Fig. 2, both for absolute and relative energies. Note that relative IPs are defined as the difference with respect to a reference, which was taken to be methane for C1s, ammonia for N1s, water for O1s, and methyl fluoride for F1s. As observed for K-edge excitation energies, the basis set quality does not significantly affect the MAD from experiments, suggesting fast basis set convergence. All functionals perform similarly, with a slight edge for the PBE flavored hybrids. The error on the absolute IPs stands at 1.35 ± 0.16 eV, which is very close to the errors observed at the K-edge. Relative IPs are remarkably well reproduced, which means that core binding energies from different systems can be reliably compared. Detailed values can be found in the supplementary material.

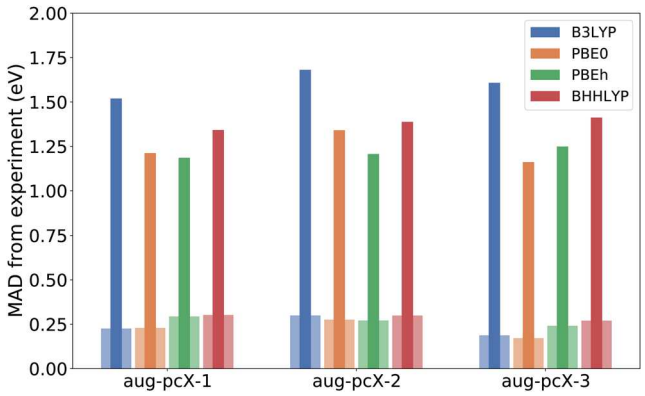

FIG. 2. Mean absolute deviation of the core 1s ionization potentials calculated with GW2X over the CORE65 benchmark set with respect to experiment. The thin dark bars represent the absolute IPs, and the wide clear bars represent the relative IPs.

In Table III, core 1s ionization potentials calculated using GW2X and similar methods from the literature are displayed. The choice of molecules is such that the overlap with other works is maximized. As discussed earlier, missing data and different basis sets only allow for a semi-quantitative comparison. It is noteworthy that B3LYP-ΔSCF performs the best, despite being the conceptually simplest method. The higher order methods' equation-of-motion CCSD, PHEh(α = 0.45)-G0W0, and transition operator electron propagator (TOEP2) yield comparable results with each other and are relatively close to B3LYP-ΔSCF. The second-order electron propagator method (EP2) and GW2X perform remarkably similarly. This is to be expected since GW2X is the DFT version of EP2, but this nonetheless underlines the validity of the generalization scheme. Despite exhibiting lower accuracy than the other methods, our implementation of GW2X still improves upon Koopmans's theorem[75] by an order of magnitude[68] while only scaling cubically. Note that the GW2X core IPs increasingly diverge from experiments with atomic number. This behavior is, however, not observed for the GW2X LR-TDDFT corrected K-edge energies of Table I, which suggests that some form of error cancellation takes place.

C. Approximations for increased efficiency

Various approximations can be employed to speed up GW2X calculations. The auxiliary density matrix method[76] under its purified (ADMM1) and non-purified flavors (ADMM2) allow for very efficient ground state hybrid functional calculations. We previously showed in Ref. 24 that such an approximate calculation can serve as a base to a LR-TDDFT perturbative treatment with only minor loss of accuracy. In this work, we further propose the ADMM method as a mean to accelerate the construction of the generalized Fock matrix, which is a necessary step of the GW2X method. In Table IV, we investigate the impact of the ADMM approximation on K-edge corrections and core IP calculations compared to the full Hartree–Fock exchange treatment. Additionally, we report the results obtained using the GW2X* method (as described in Sec. II) and the non-core-specific aug-pcseg[77]/aug-admm[78] basis sets. There is practically no

TABLE III. Comparison of GW2X 1s core ionization potentials with similar methods from the literature. The difference between the calculated and experimental IP is reported (in eV). The bold atom in the chemical formula is the one being ionized.

	B3LYP-ΔSCF[33] u6-311G**	PBEh-G0W0[67] cc-pVQZ	EOM-CCSD[36] aug-cc-pVTZ	EP2[68] cc-pVTZ	TOEP2[68] cc-pVTZ	PBEh-GW2X aug-pcX-2	Expt.
CH_4	+0.17	−0.44	···	+0.75	+0.31	+0.09	290.84[69]
C_2H_4	···	−0.28	+0.39	+0.99	+1.37	+0.18	290.82[69]
CO	+0.51	−0.65	+0.45	+1.74	+1.10	+0.91	296.23[69]
CH_2O	+0.31	−0.11	···	+1.59	+0.93	+0.76	294.38[70]
NH_3	−0.01	−0.61	+0.60	···	···	−1.04	405.52[70]
NNO	+0.21	···	···	+0.29	+0.44	−1.04	408.66[71]
N**N**O	+0.24	···	···	+0.75	+1.76	−0.57	412.57[71]
C**O**	+0.33	−0.92	+1.33	−0.93	−0.24	−2.17	542.10[72]
H_2**O**	−0.41	−1.30	+0.75	−2.02	−0.42	−2.48	539.90[71]
CH_2**O**	−0.19	−1.12	···	−1.93	−0.83	−2.27	539.33[70]
H**F**	−0.45	···	···	−3.44	−0.98	−3.55	694.18[71]
F_2	−0.38	···	···	−2.42	−1.28	−3.02	696.69[71]
MAD	0.29	0.68	0.70	1.53	0.88	1.51	

difference in accuracy between the two ADMM schemes, making the more efficient non-purified version the default choice. Compared to full HFX, ADMM introduces an additional error of 0.2–0.3 eV for GW2X K-edge correction and 0.4–0.5 eV for core IPs. The error is increased when ADMM is used together with the more approximate GW2X* scheme, especially for IP calculations. It is noteworthy that the use of the general purpose aug-pcseg-2 and corresponding aug-admm-2 basis sets do not greatly change the results, suggesting that large core-specific basis sets are not strictly necessary in this context. This is particularly useful for making large scale calculations more affordable. Finally, the errors induced by the ADMM and/or GW2X* approximations at the K-edge are rather small compared to the scale of a near-edge x-ray absorption spectrum, which typically spans 15–20 eV.

D. GW2X in extended systems

There is, in principle, no issue with using GW2X as a correction scheme in periodic boundary conditions (PBCs). Moreover, the high levels of symmetry found in crystal structures can be exploited for efficiency. Since multiple atoms are equivalent, it is only necessary to correct the core KS eigenvalue for one of those, leading to a $\mathcal{O}(n^3)$ scaling with system size. Note that disordered systems such as liquids are limited to a $\mathcal{O}(n^4)$ scaling, as each atom may have a slightly different environment. GW2X being related to second-order Møller–Plesset perturbation theory,[82] it suffers from the same limitations. In particular, it works best for large gap molecular systems, whereas semiconductors require large supercells for converged results.[83]

TABLE IV. Mean average deviation (in eV) of the GW2X method with respect to experiments, using various approximations. The same benchmark sets as for Figs. 1 and 2 were used for K-edge and core ionization potentials, respectively. The PBEh(α = 0.45) functional and the aug-pcX-2/aug-admm-2 and aug-pcseg-2/aug-admm-2 basis set combinations were used. The results within parentheses refer to the latter.

	K-edge		IP	
	GW2X	GW2X*	GW2X	GW2X*
Full HFX	1.2 (1.2)	1.3 (1.2)	1.2 (1.0)	1.6 (1.6)
ADMM1	1.4 (1.3)	1.6 (1.4)	1.6 (1.4)	2.2 (1.8)
ADMM2	1.5 (1.3)	1.6 (1.5)	1.7 (1.4)	2.2 (1.9)

We applied the GW2X correction schemes on three molecular crystals, namely, solid ammonia, ice 1h, and solid argon. The respective unit cells contain 128, 288, and 32 atoms, and the structures were first relaxed at the DZVP-MOLOPT-SR-GTH[84]/PBE[85]+D3[86] level of theory. LR-TDDFT+GW2X calculations were then performed using the PBEh(α = 0.45) hybrid functional with the truncated Coulomb potential[87] (truncation radii of 5, 6, and 5 Å, i.e., just under half of the cell parameter). The corrected LR-TDDFT spectra are shown in Fig. 3. The first two absorption peaks of crystalline NH_3 are well aligned to the experimental spectrum, thanks to the GW2X correction that amounts to a blue shift of 3.7 eV. The relative intensity of the first peak is too small, but this issue lies with LR-TDDFT rather than the correction scheme. The triple zeta aug-pceseg-2/aug-admm-2 basis sets were used to describe a single excited nitrogen atom, while all other atoms relied on GTH pseudopotentials[88–90] and DZVP-MOLOPT-SR-GTH/FIT3[76] basis sets. The hexagonal ice spectrum was calculated using the same basis sets, where only one excited oxygen atom was described at the all-electron level as well. The GW2X correction to the spectrum is a blue shift of 2.8 eV, which also aligns the first few peaks remarkably well. The relative intensities are, however, quite poor, and the reasons will be discussed later. The solid argon simulated spectrum is well aligned (GW2X shift of 3.5 eV) and enjoys good relative intensities. Using the higher quality quadruple zeta aug-pcseg-3 was found to be necessary, and the added diffuse functions of the augmented set were found to be especially crucial. Only one atom was described at the all-electron level and all others using DZVP-MOLOPT-SR-GTH basis sets. However, since there is no available auxiliary FIT3 basis set for argon, full HFX was employed instead of the ADMM approximation. Note that using

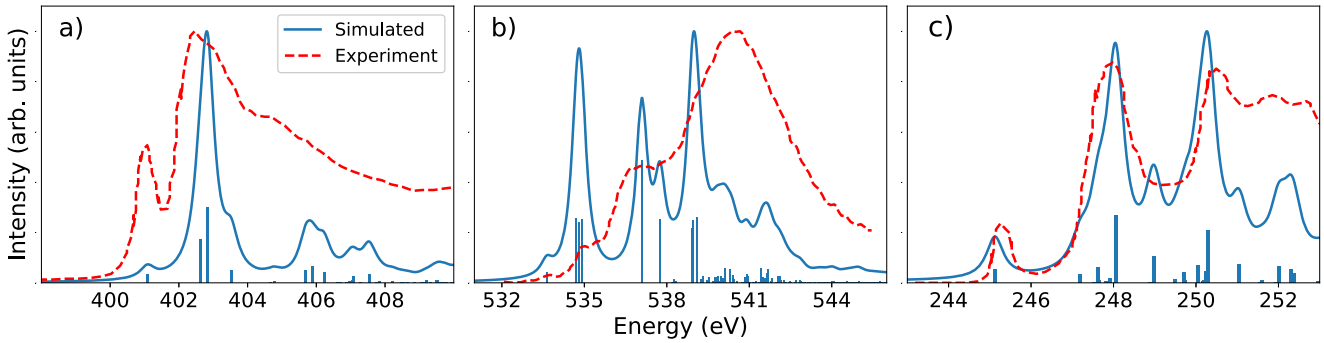

FIG. 3. GW2X corrected LR-TDDFT spectra of (a) the solid ammonia N K-edge, (b) the ice 1h O K-edge, and (c) the solid argon Ar $L_{2,3}$-edge in periodic boundary conditions. The PBEh(α = 0.45) functional and a mix of all electron basis sets and pseudopotentials were used. The GW2X corrections amount to blue shifts of 3.7, 2.8, and 3.5 eV for ammonia, ice, and argon, respectively. A Lorentzian broadening of fwhm 0.5 eV was applied, and calculated intensities were uniformly scaled to match experiments. Experimental data come from Refs. 79–81.

quadruple zeta basis sets for ammonia and ice did not improve the results.

Most of the efficiency aimed approximations discussed in Sec. III C were used in our extended system calculations. General purpose aug-pcseg basis sets were used throughout as was the non-purified ADMM scheme for solid NH_3 and ice 1h. Moreover, only one atom per system was described at the all-electron level, while all others relied on pseudopotentials, essentially freezing their core and reducing the number of MOs to include in Eq. (13). Only the original GW2X scheme was preferred over the simplified GW2X* version as the systems are too small for notable efficiency gains. The spectra obtained with the latter method are available in the supplementary material. Note that a truncated Coulomb potential was used for exact exchange integrals in order to avoid nonphysical self-exchange.[87] The same operator was used for ground state HFX, LR-TDDFT exact exchange kernel, and thus also GW2X. The use of such a short range exchange operator also reduces the cost and scaling of the previously mentioned integrals. We did not observe a dependence of the GW2X results on truncation radius, provided that it is large enough (5–6 Å). To illustrate the overall affordability of the method, all calculations were run on a 24 CPU core system and execution times reported in Fig. 4. The ground state SCF calculation dominates overall, mostly because of the ERIs evaluation for the HFX fraction of the functional. This is so even with the initial SCF guess coming from a converged PBE calculation and the ADMM approximation for ammonia and ice. The efficiency of the GW2X correction is emphasized by the fact that it takes at most 60% of the post-SCF effort in ice, and is almost negligible for the other two smaller systems. The most expensive calculation, solid argon, ran with a wall time of just under 40 min.

As previously mentioned, while the spectral features of the hexagonal ice spectrum are well aligned with experimental data, the relative intensities are unsatisfactory. Based on TP-DFT[91] and CPP-DFT[92,93] simulations, Zhovtobriukh *et al.*[94] have suggested that available ice 1h XANES spectra are not fully representative of the pristine crystal structure. Instead, they show that significant disorder around the lattice positions must be introduced to reproduce experiments. Using the GenIce[95] code, we generated a 384-atom disordered model based on hexagonal ice, with Gaussian noise applied to the position of all water molecules (the –add_noise parameter of GenIce was set to 1.0). The simulated spectrum, displayed in Fig. 5, improves upon that obtained with the pristine 1h structure. In particular, the initially very sharp first peak is broadened and decreases in relative intensity.

In periodic systems, GW2X cannot be directly used to calculate absolute binding energies. Because the potential reference can be arbitrarily defined, whereas it goes to zero far away in the non-periodic case, KS eigenvalues may be uniformly shifted. Thus, the solution of Eq. (13) for the IP will be shifted by some unknown amount in PBCs. However, once plugged into Eq. (12) for the LR-TDDFT correction, the shifts cancel out. A possible way to calculate core IPs in PBCs using GW2X would be to use slab models and reference the KS eigenvalues against the vacuum level, as it is done in the *GW* community.[96–98]

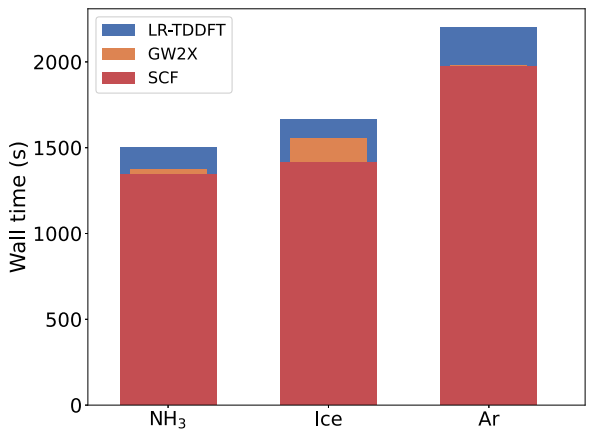

FIG. 4. Execution times of the extended system calculations of Fig. 3. All calculations were carried out on an Intel S2600WT2R machine with 24 CPUs and 256 GB of memory. Different colors represent the time spent treating the ground state SCF, the LR-TDDFT equations, and the GW2X correction. Note that the time spent evaluating the AOs' RI integrals shared by GW2X and LR-TDDFT is credited to the latter.

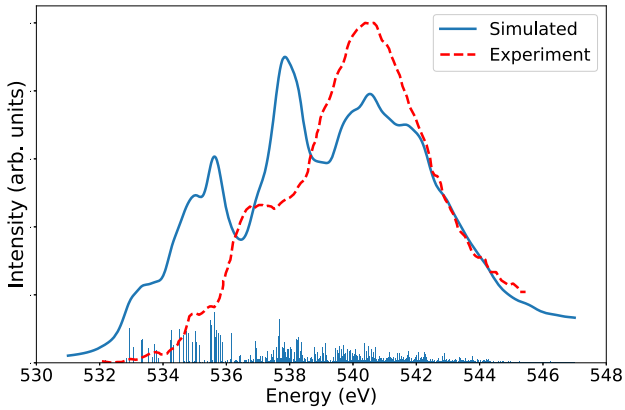

FIG. 5. Hexagonal ice XANES spectrum calculated based on a perturbed crystal structure obtained with the GenIce code. The model contains 384 atoms, 8 of which (all oxygen atoms) were randomly selected to be excited. The choice of functional and basis sets is the same as for Fig. 3. The GW2X shift amounts to 3.4 ± 0.1 eV.

IV. CONCLUSION

We have implemented a correction scheme to address the lack of orbital relaxation and the self-interaction error that afflicts the prediction of absolute excitation energies in LR-TDDFT for core level spectroscopy. The methods are based on the DFT generalization of the second-order electron propagator theory (GW2X). It allows for the accurate calculation of ionization potentials, which are then substituted into the LR-TDDFT equations, replacing the KS eigenvalues. The implementation exploits the local nature of core states for efficiency, scaling cubically with system size and integrating seamlessly in our existing core level LR-TDDFT implementation.

Benchmarks at the K- and L-edges show that the GW2X correction scheme systematically improves LR-TDDFT results for four common hybrid functionals, namely, B3LYP, PBE0, PBEh($\alpha = 0.45$), and BHHLYP, reaching accuracies comparable to higher level methods, such as the equation of motion CCSD. Moreover, the method can be used to calculate core ionization potentials directly with similar errors to those observed at the K-edge. Rapid basis set convergence was observed in both LR-TDDFT correction and core binding energy calculation, and the use of core-specific basis sets does not seem essential.

The method is applicable with periodic boundary conditions for large gap molecular systems, as demonstrated for solid ammonia, ice 1h, and crystalline argon. Such calculations are accessible with modest computer resources and are made feasible due to efficient approximations. In particular, mixing the ADMM scheme and a hybrid all-electron/pseudopotential description has proven effective. Core ionization potentials are, however, not easily accessible in such systems and would require additional calculations.

This work focuses on standard GW2X, and there is room for further exploration. The initial GW2X paper[48] also describes the GW(2) approach, which could prove more efficient since the exchange contributions are ignored. Alternatively, the accuracy could potentially be improved by using spin scaling approaches, as done in SCS- and SOS-MP2.[99,100]

SUPPLEMENTARY MATERIAL

The supplementary material contains tables with the detailed values of the K-edge and ionization potential benchmarks as well as related figures augmented with pure Hartree–Fock results. It also contains simulated XANES spectra of solid ammonia, ice 1h, and solid argon corrected with the approximate GW2X* method.

ACKNOWLEDGMENTS

This work was supported by the MARVEL National Centre for Competency in Research funded by the Swiss National Science Foundation (Grant Agreement ID 51NF40-182892).

DATA AVAILABILITY

The data that support the findings of this study are openly available in the Materials Cloud at http://doi.org/10.24435/materialscloud:1e-b4.

REFERENCES

[1]M. E. Casida, "Time-dependent density functional response theory for molecules," in *Recent Advances in Density Functional Methods, Part I* (World Scientific, 1995), pp. 155–192.
[2]K. Yabana and G. F. Bertsch, "Time-dependent local-density approximation in real time," Phys. Rev. B **54**, 4484 (1996).
[3]L. S. Cederbaum, W. Domcke, and J. Schirmer, "Many-body theory of core holes," Phys. Rev. A **22**, 206 (1980).
[4]K. Lopata, B. E. van Kuiken, M. Khalil, and N. Govind, "Linear-response and real-time time-dependent density functional theory studies of core-level near-edge X-ray absorption," J. Chem. Theory Comput. **8**, 3284–3292 (2012).
[5]M. Stener, G. Fronzoni, and M. de Simone, "Time dependent density functional theory of core electrons excitations," Chem. Phys. Lett. **373**, 115–123 (2003).
[6]N. A. Besley and A. Noble, "Time-dependent density functional theory study of the X-ray absorption spectroscopy of acetylene, ethylene, and benzene on Si(100)," J. Phys. Chem. C **111**, 3333–3340 (2007).
[7]S. DeBeer George, T. Petrenko, and F. Neese, "Time-dependent density functional calculations of ligand K-edge X-ray absorption spectra," Inorg. Chim. Acta **361**, 965–972 (2008).
[8]W. Liang, S. A. Fischer, M. J. Frisch, and X. Li, "Energy-specific linear response TDHF/TDDFT for calculating high-energy excited states," J. Chem. Theory Comput. **7**, 3540–3547 (2011).
[9]N. Schmidt, R. Fink, and W. Hieringer, "Assignment of near-edge x-ray absorption fine structure spectra of metalloporphyrins by means of time-dependent density-functional calculations," J. Chem. Phys. **133**, 054703 (2010).
[10]N. A. Besley, "Modeling of the spectroscopy of core electrons with density functional theory," Wiley Interdiscip. Rev.: Comput. Mol. Sci. **2021**, e1527.
[11]Y. Imamura and H. Nakai, "Analysis of self-interaction correction for describing core excited states," Int. J. Quantum Chem. **107**, 23–29 (2007).
[12]S. G. Minasian, J. M. Keith, E. R. Batista, K. S. Boland, D. L. Clark, S. A. Kozimor, R. L. Martin, D. K. Shuh, and T. Tyliszczak, "New evidence for 5f covalency in actinocenes determined from carbon K-edge XAS and electronic structure theory," Chem. Sci. **5**, 351–359 (2014).
[13]A. Nardelli, G. Fronzoni, and M. Stener, "Theoretical study of sulfur L-edge XANES of thiol protected gold nanoparticles," Phys. Chem. Chem. Phys. **13**, 480–487 (2011).
[14]C. Li, P. Salén, V. Yatsyna, L. Schio, R. Feifel, R. Squibb, M. Kamińska, M. Larsson, R. Richter, M. Alagia *et al.*, "Experimental and theoretical XPS and NEXAFS studies of *N*-methylacetamide and *N*-methyltrifluoroacetamide," Phys. Chem. Chem. Phys. **18**, 2210–2218 (2016).
[15]S. DeBeer George and F. Neese, "Calibration of scalar relativistic density functional theory for the calculation of sulfur K-edge X-ray absorption spectra," Inorg. Chem. **49**, 1849–1853 (2010).

[16]V. Martin-Diaconescu, M. Gennari, B. Gerey, E. Tsui, J. Kanady, R. Tran, J. Pécaut, D. Maganas, V. Krewald, E. Gouré *et al.*, "Ca K-edge XAS as a probe of calcium centers in complex systems," Inorg. Chem. **54**, 1283–1292 (2015).
[17]P. Norman and A. Dreuw, "Simulating X-ray spectroscopies and calculating core-excited states of molecules," Chem. Rev. **118**, 7208–7248 (2018).
[18]G. Tu, Z. Rinkevicius, O. Vahtras, H. Ågren, U. Ekström, P. Norman, and V. Carravetta, "Self-interaction-corrected time-dependent density-functional-theory calculations of x-ray-absorption spectra," Phys. Rev. A **76**, 022506 (2007).
[19]A. Nakata, Y. Imamura, and H. Nakai, "Hybrid exchange-correlation functional for core, valence, and Rydberg excitations: Core-valence-Rydberg B3LYP," J. Chem. Phys. **125**, 064109 (2006).
[20]J.-W. Song, M. A. Watson, A. Nakata, and K. Hirao, "Core-excitation energy calculations with a long-range corrected hybrid exchange-correlation functional including a short-range Gaussian attenuation (LCgau-BOP)," J. Chem. Phys. **129**, 184113 (2008).
[21]N. A. Besley, M. J. G. Peach, and D. J. Tozer, "Time-dependent density functional theory calculations of near-edge X-ray absorption fine structure with short-range corrected functionals," Phys. Chem. Chem. Phys. **11**, 10350–10358 (2009).
[22]E. van Lenthe, E. J. Baerends, and J. G. Snijders, "Relativistic regular two-component Hamiltonians," J. Chem. Phys. **99**, 4597–4610 (1993).
[23]B. A. Hess, "Relativistic electronic-structure calculations employing a two-component no-pair formalism with external-field projection operators," Phys. Rev. A **33**, 3742 (1986).
[24]A. Bussy and J. Hutter, "Efficient and low-scaling linear-response time-dependent density functional theory implementation for core-level spectroscopy of large and periodic systems," Phys. Chem. Chem. Phys. **23**, 4736–4746 (2021).
[25]T. D. Kühne, M. Iannuzzi, M. Del Ben, V. V. Rybkin, P. Seewald, F. Stein, T. Laino, R. Z. Khaliullin, O. Schütt, F. Schiffmann *et al.*, "CP2K: An electronic structure and molecular dynamics software package—Quickstep: Efficient and accurate electronic structure calculations," J. Chem. Phys. **152**, 194103 (2020).
[26]R. Sternheimer, "On nuclear quadrupole moments," Phys. Rev. **84**, 244 (1951).
[27]J. Hutter, "Excited state nuclear forces from the Tamm–Dancoff approximation to time-dependent density functional theory within the plane wave basis set framework," J. Chem. Phys. **118**, 3928–3934 (2003).
[28]E. Gross and W. Kohn, "Time-dependent density-functional theory," Adv. Quantum Chem. **21**, 255 (1990).
[29]S. Hirata and M. Head-Gordon, "Time-dependent density functional theory within the Tamm–Dancoff approximation," Chem. Phys. Lett. **314**, 291–299 (1999).
[30]A. L. Fetter and J. D. Walecka, *Quantum Theory of Many-Particle Systems* (Courier Corporation, 2012).
[31]N. A. Besley, "Fast time-dependent density functional theory calculations of the X-ray absorption spectroscopy of large systems," J. Chem. Theory Comput. **12**, 5018–5025 (2016).
[32]J. J. Rehr, E. A. Stern, R. L. Martin, and E. R. Davidson, "Extended x-ray-absorption fine-structure amplitudes—Wave-function relaxation and chemical effects," Phys. Rev. B **17**, 560 (1978).
[33]N. A. Besley, A. T. B. Gilbert, and P. M. W. Gill, "Self-consistent-field calculations of core excited states," J. Chem. Phys. **130**, 124308 (2009).
[34]D. Hait and M. Head-Gordon, "Highly accurate prediction of core spectra of molecules at density functional theory cost: Attaining sub-electronvolt error from a restricted open-shell Kohn–Sham approach," J. Phys. Chem. Lett. **11**, 775–786 (2020).
[35]F. A. Asmuruf and N. A. Besley, "Calculation of near-edge X-ray absorption fine structure with the CIS(D) method," Chem. Phys. Lett. **463**, 267–271 (2008).
[36]M. L. Vidal, X. Feng, E. Epifanovsky, A. I. Krylov, and S. Coriani, "New and efficient equation-of-motion coupled-cluster framework for core-excited and core-ionized states," J. Chem. Theory Comput. **15**, 3117–3133 (2019).
[37]J. Schirmer, A. B. Trofimov, K. J. Randall, J. Feldhaus, A. M. Bradshaw, Y. Ma, C. T. Chen, and F. Sette, "K-shell excitation of the water, ammonia, and methane molecules using high-resolution photoabsorption spectroscopy," Phys. Rev. A **47**, 1136 (1993).
[38]A. P. Hitchcock and C. E. Brion, "Carbon K-shell excitation of C_2H_2, C_2H_4, C_2H_6 and C_6H_6 by 2.5 keV electron impact," J. Electron Spectrosc. Relat. Phenom. **10**, 317–330 (1977).
[39]M. Domke, C. Xue, A. Puschmann, T. Mandel, E. Hudson, D. A. Shirley, and G. Kaindl, "Carbon and oxygen K-edge photoionization of the CO molecule," Chem. Phys. Lett. **173**, 122–128 (1990).
[40]G. Remmers, M. Domke, A. Puschmann, T. Mandel, C. Xue, G. Kaindl, E. Hudson, and D. A. Shirley, "High-resolution *K*-shell photoabsorption in formaldehyde," Phys. Rev. A **46**, 3935 (1992).
[41]K. C. Prince, L. Avaldi, M. Coreno, R. Camilloni, and M. de Simone, "Vibrational structure of core to Rydberg state excitations of carbon dioxide and dinitrogen oxide," J. Phys. B: At., Mol. Opt. Phys. **32**, 2551 (1999).
[42]A. P. Hitchcock and C. E. Brion, "K-shell excitation of HF and F_2 studied by electron energy-loss spectroscopy," J. Phys. B: At. Mol. Phys. **14**, 4399 (1981).
[43]C. A. Ullrich, *Time-Dependent Density-Functional Theory: Concepts and Applications* (OUP Oxford, 2011).
[44]I. Dabo, A. Ferretti, N. Poilvert, Y. Li, N. Marzari, and M. Cococcioni, "Koopmans' condition for density-functional theory," Phys. Rev. B **82**, 115121 (2010).
[45]P. Verma and R. J. Bartlett, "Increasing the applicability of density functional theory. V. X-ray absorption spectra with ionization potential corrected exchange and correlation potentials," J. Chem. Phys. **145**, 034108 (2016).
[46]L. S. Cederbaum, "Direct calculation of ionization potentials of closed-shell atoms and molecules," Theor. Chim. Acta **31**, 239–260 (1973).
[47]J. V. Ortiz, "Electron propagator theory: An approach to prediction and interpretation in quantum chemistry," Wiley Interdiscip. Rev.: Comput. Mol. Sci. **3**, 123–142 (2013).
[48]Y. Shigeta, A. M. Ferreira, V. G. Zakrzewski, and J. V. Ortiz, "Electron propagator calculations with Kohn–Sham reference states," Int. J. Quantum Chem. **85**, 411–420 (2001).
[49]B. T. Pickup and O. Goscinski, "Direct calculation of ionization energies: I. Closed shells," Mol. Phys. **26**, 1013–1035 (1973).
[50]M. L. Vidal, P. Pokhilko, A. I. Krylov, and S. Coriani, "Equation-of-motion coupled-cluster theory to model L-edge X-ray absorption and photoelectron spectra," J. Phys. Chem. Lett. **11**, 8314–8321 (2020).
[51]W. Hayes and F. C. Brown, "Absorption by some molecular gases in the extreme ultraviolet," Phys. Rev. A **6**, 21 (1972).
[52]J. D. Bozek, K. H. Tan, G. M. Bancroft, and J. S. Tse, "High resolution gas phase photoabsorption spectra of $SiCl_4$ and $Si(CH_3)_4$ at the silicon l-edges: Characterization and assignment of resonances," Chem. Phys. Lett. **138**, 33–42 (1987).
[53]Z. F. Liu, J. N. Cutler, G. M. Bancroft, K. H. Tan, R. G. Cavell, and J. S. Tse, "High resolution gas phase photoabsorption spectra and multiple-scattering Xα study of PX_3(X = H, CH_3, CF_3) compounds at the P $L_{2,3}$ edge," Chem. Phys. Lett. **172**, 421–429 (1990).
[54]J. J. Neville, A. Jürgensen, R. G. Cavell, N. Kosugi, and A. P. Hitchcock, "Inner-shell excitation of PF_3, PCl_3, PCl_2CF_3, OPF_3 and SPF_3: Part I. Spectroscopy," Chem. Phys. **238**, 201–220 (1998).
[55]R. Guillemin, W. C. Stolte, L. T. N. Dang, S.-W. Yu, and D. W. Lindle, "Fragmentation dynamics of H_2S following S 2*p* photoexcitation," J. Chem. Phys. **122**, 094318 (2005).
[56]U. Ankerhold, B. Esser, and F. Von Busch, "Ionization and fragmentation of OCS and CS_2 after photoexcitation around the sulfur 2p edge," Chem. Phys. **220**, 393–407 (1997).
[57]A. Krasnoperova, E. Gluskin, L. Mazalov, and V. Kochubei, "The fine structure of the $l_{II,III}$ absorption edge of sulfur in the SO_2 molecule," J. Struct. Chem. **17**, 947–950 (1976).
[58]H. Aksela, S. Aksela, M. Ala-Korpela, O.-P. Sairanen, M. Hotokka, G. M. Bancroft, K. H. Tan, and J. Tulkki, "Decay channels of core-excited HCl," Phys. Rev. A **41**, 6000 (1990).
[59]O. Nayandin, E. Kukk, A. Wills, B. Langer, J. Bozek, S. Canton-Rogan, M. Wiedenhoeft, D. Cubaynes, and N. Berrah, "Angle-resolved two-dimensional mapping of electron emission from the inner-shell 2p excitations in Cl_2," Phys. Rev. A **63**, 062719 (2001).

[60]U. Borštnik, J. VandeVondele, V. Weber, and J. Hutter, "Sparse matrix multiplication: The distributed block-compressed sparse row library," Parallel Comput. **40**, 47–58 (2014).
[61]F. Weigend and R. Ahlrichs, "Balanced basis sets of split valence, triple zeta valence and quadruple zeta valence quality for H to Rn: Design and assessment of accuracy," Phys. Chem. Chem. Phys. **7**, 3297–3305 (2005).
[62]P. J. Stephens, F. J. Devlin, C. F. Chabalowski, and M. J. Frisch, "Ab initio calculation of vibrational absorption and circular dichroism spectra using density functional force fields," J. Phys. Chem. **98**, 11623–11627 (1994).
[63]M. A. Ambroise and F. Jensen, "Probing basis set requirements for calculating core ionization and core excitation spectroscopy by the Δ self-consistent-field approach," J. Chem. Theory Comput. **15**, 325–337 (2018).
[64]C. Adamo and V. Barone, "Toward reliable density functional methods without adjustable parameters: The PBE0 model," J. Chem. Phys. **110**, 6158–6170 (1999).
[65]V. Atalla, M. Yoon, F. Caruso, P. Rinke, and M. Scheffler, "Hybrid density functional theory meets quasiparticle calculations: A consistent electronic structure approach," Phys. Rev. B **88**, 165122 (2013).
[66]A. D. Becke, "A new mixing of Hartree–Fock and local density-functional theories," J. Chem. Phys. **98**, 1372–1377 (1993).
[67]D. Golze, L. Keller, and P. Rinke, "Accurate absolute and relative core-level binding energies from *GW*," J. Phys. Chem. Lett. **11**, 1840–1847 (2020).
[68]R. Flores-Moreno, V. G. Zakrzewski, and J. V. Ortiz, "Assessment of transition operator reference states in electron propagator calculations," J. Chem. Phys. **127**, 134106 (2007).
[69]V. Myrseth, J. D. Bozek, E. Kukk, L. J. Sæthre, and T. D. Thomas, "Adiabatic and vertical carbon 1s ionization energies in representative small molecules," J. Electron Spectrosc. Relat. Phenom. **122**, 57–63 (2002).
[70]A. A. Bakke, H.-W. Chen, and W. L. Jolly, "A table of absolute core-electron binding-energies for gaseous atoms and molecules," J. Electron Spectrosc. Relat. Phenom. **20**, 333–366 (1980).
[71]W. L. Jolly, K. D. Bomben, and C. J. Eyermann, "Core-electron binding energies for gaseous atoms and molecules," At. Data Nucl. Data Tables **31**, 433–493 (1984).
[72]K. Siegbahn, *ECSA Applied to Free Molecules* (North-Holland Publishing, 1969).
[73]D. Hait and M. Head-Gordon, "Excited state orbital optimization via minimizing the square of the gradient: General approach and application to singly and doubly excited states via density functional theory," J. Chem. Theory Comput. **16**, 1699–1710 (2020).
[74]J. Sun, A. Ruzsinszky, and J. P. Perdew, "Strongly constrained and appropriately normed semilocal density functional," Phys. Rev. Lett. **115**, 036402 (2015).
[75]T. Koopmans, "Über die zuordnung von wellenfunktionen und eigenwerten zu den einzelnen elektronen eines atoms," Physica **1**, 104–113 (1934).
[76]M. Guidon, J. Hutter, and J. VandeVondele, "Auxiliary density matrix methods for Hartree–Fock exchange calculations," J. Chem. Theory Comput. **6**, 2348–2364 (2010).
[77]F. Jensen, "Unifying general and segmented contracted basis sets. Segmented polarization consistent basis sets," J. Chem. Theory Comput. **10**, 1074–1085 (2014).
[78]C. Kumar, H. Fliegl, F. Jensen, A. M. Teale, S. Reine, and T. Kjaergaard, "Accelerating Kohn-Sham response theory using density fitting and the auxiliary-density-matrix method," Int. J. Quantum Chem. **118**, e25639 (2018).
[79]P. Parent, F. Bournel, J. Lasne, S. Lacombe, G. Strazzulla, S. Gardonio, S. Lizzit, J.-P. Kappler, L. Joly, C. Laffon *et al.*, "The irradiation of ammonia ice studied by near edge x-ray absorption spectroscopy," J. Chem. Phys. **131**, 154308 (2009).
[80]P. Wernet, D. Nordlund, U. Bergmann, M. Cavalleri, M. Odelius, H. Ogasawara, L.-Å. Näslund, T. Hirsch, L. Ojamäe, P. Glatzel *et al.*, "The structure of the first coordination shell in liquid water," Science **304**, 995–999 (2004).
[81]R. Haensel, G. Keitel, N. Kosuch, U. Nielsen, and P. Schreiber, "Optical absorption of solid neon and argon in the soft x-ray region," J. Phys. Colloq. **32**, C4-236 (1971).
[82]C. Møller and M. S. Plesset, "Note on an approximation treatment for many-electron systems," Phys. Rev. **46**, 618 (1934).
[83]T. Gruber, K. Liao, T. Tsatsoulis, F. Hummel, and A. Grüneis, "Applying the coupled-cluster ansatz to solids and surfaces in the thermodynamic limit," Phys. Rev. X **8**, 021043 (2018).
[84]J. VandeVondele and J. Hutter, "Gaussian basis sets for accurate calculations on molecular systems in gas and condensed phases," J. Chem. Phys. **127**, 114105 (2007).
[85]J. P. Perdew, K. Burke, and M. Ernzerhof, "Generalized gradient approximation made simple," Phys. Rev. Lett. **77**, 3865 (1996).
[86]S. Grimme, J. Antony, S. Ehrlich, and H. Krieg, "A consistent and accurate *ab initio* parametrization of density functional dispersion correction (DFT-D) for the 94 elements H-Pu," J. Chem. Phys. **132**, 154104 (2010).
[87]M. Guidon, J. Hutter, and J. VandeVondele, "Robust periodic Hartree–Fock exchange for large-scale simulations using Gaussian basis sets," J. Chem. Theory Comput. **5**, 3010–3021 (2009).
[88]S. Goedecker, M. Teter, and J. Hutter, "Separable dual-space Gaussian pseudopotentials," Phys. Rev. B **54**, 1703 (1996).
[89]C. Hartwigsen, S. Goedecker, and J. Hutter, "Relativistic separable dual-space Gaussian pseudopotentials from H to Rn," Phys. Rev. B **58**, 3641 (1998).
[90]M. Krack, "Pseudopotentials for H to Kr optimized for gradient-corrected exchange-correlation functionals," Theor. Chem. Acc. **114**, 145–152 (2005).
[91]L. Triguero, L. G. M. Pettersson, and H. Ågren, "Calculations of near-edge x-ray-absorption spectra of gas-phase and chemisorbed molecules by means of density-functional and transition-potential theory," Phys. Rev. B **58**, 8097 (1998).
[92]U. Ekström and P. Norman, "X-ray absorption spectra from the resonant-convergent first-order polarization propagator approach," Phys. Rev. A **74**, 042722 (2006).
[93]U. Ekström, P. Norman, V. Carravetta, and H. Ågren, "Polarization propagator for x-ray spectra," Phys. Rev. Lett. **97**, 143001 (2006).
[94]I. Zhovtobriukh, P. Norman, and L. G. M. Pettersson, "X-ray absorption spectrum simulations of hexagonal ice," J. Chem. Phys. **150**, 034501 (2019).
[95]M. Matsumoto, T. Yagasaki, and H. Tanaka, "GenIce: Hydrogen-disordered ice generator," J. Comput. Chem. **39**, 61 (2018).
[96]W. Chen and A. Pasquarello, "Band-edge positions in *GW*: Effects of starting point and self-consistency," Phys. Rev. B **90**, 165133 (2014).
[97]T. A. Pham, C. Zhang, E. Schwegler, and G. Galli, "Probing the electronic structure of liquid water with many-body perturbation theory," Phys. Rev. B **89**, 060202 (2014).
[98]Y. Hinuma, A. Grüneis, G. Kresse, and F. Oba, "Band alignment of semiconductors from density-functional theory and many-body perturbation theory," Phys. Rev. B **90**, 155405 (2014).
[99]S. Grimme, "Accurate calculation of the heats of formation for large main group compounds with spin-component scaled MP2 methods," J. Phys. Chem. A **109**, 3067–3077 (2005).
[100]Y. Jung, R. C. Lochan, A. D. Dutoi, and M. Head-Gordon, "Scaled opposite-spin second order Møller–Plesset correlation energy: An economical electronic structure method," J. Chem. Phys. **121**, 9793–9802 (2004).